

The Lightest Massive Invisible Particles at the LHC

André de Gouvêa and Andrew C. Kobach

Northwestern University, Department of Physics & Astronomy, 2145 Sheridan Road, Evanston, IL 60208, USA

(Dated: October 1, 2012)

The observation of new physics events with large missing transverse energy at the LHC would potentially serve as evidence for the direct production dark matter. A crucial step toward verifying such evidence is the measurement of the would-be dark matter mass. If, for example, the invisible particles are found to have masses consistent with zero, it may prove very challenging to ascertain whether light dark matter or neutrinos are being observed. We assume that new invisible particles are pair-produced in a $t\bar{t}$ -like topology and use two M_{T2} -based methods to measure the masses of the particles associated with the missing energy. We find that if the uncertainty associated with measuring the M_{T2} endpoints is $\mathcal{O}(1 \text{ GeV})$, the invisible particles must have masses greater than $\mathcal{O}(10 \text{ GeV})$ so they can be distinguished from massless ones. In general, the uncertainty associated with measuring the mass of the invisible particles increases as the mass decreases. If the recent results from the CoGeNT, DAMA/LIBRA, and CRESST experiments have indeed revealed the existence of light dark matter, our results suggest that it may be difficult for the LHC to distinguish dark matter from neutrinos solely via mass measurements.

I. INTRODUCTION

One of the main goals of high energy accelerator experiments like the LHC is the discovery, via direct production and subsequent detection of the associated decay products, of degrees of freedom beyond those present in the standard model. An advantage of direct production is that the various properties of the new particles, including their masses, can be measured, often with very good precision. Different methods exist for measuring the masses of the particles involved in different production and decay topologies [1, 2], but a unique problem arises when one or more of the final-state particles are “invisible,” i.e., they do not interact directly with the detector. At a hadron collider, the existence of invisible particles can be inferred only via momentum conservation in the plane transverse to the beamline; only the vector sum of the transverse momenta associated with invisible particles can be reconstructed. If two missing particles in a single event each originate from identical decay chains, e.g., a $t\bar{t}$ -like topology¹, the M_{T2} variable [3] is a useful tool for extracting the masses of the parent, intermediate, and invisible particles in the decay chain. Remarkably, this includes the mass of the particles associated with the missing energy in the event [4–7].

Two popular M_{T2} -based methods for extracting the masses of the particles in a $t\bar{t}$ -like decay topology are reconstructing the M_{T2} kink [4–6] and the M_{T2} subsystems method [7]. The M_{T2} kink method involves measuring M_{T2} endpoints, which we call M_{T2}^{\max} , for different values of an ansatz for the invisible particles’ mass [4–6]. Analytical expressions can be fit to the distribution of M_{T2}^{\max} as a function of the input ansatz, and the masses of the particles in the decay chain can be determined simultaneously from this fit. A kink exists in the M_{T2}^{\max} distribution at the mass of the invisible particles, but as the mass of the invisible particles becomes light, it may be difficult to determine that the location of the kink is non-zero, given experimental uncertainties. Another M_{T2} -based method involves studying M_{T2} subsystems and measuring three kinematic endpoints [7]. With the analytical expressions for the endpoints of each subsystem, one can simultaneously solve for the masses of the particles in the decay chain. If the mass of the invisible particle is light, the uncertainty for solving for its mass can become large. Because of the experimental uncertainties associated with these M_{T2} methods, there is a minimum mass of the invisible particle above which it can be distinguished from a massless particle at 95% C.L.

Much of the literature to date uses SUSY models when addressing mass determination with M_{T2} methods, taking the LSP to be $\mathcal{O}(100 \text{ GeV})$ [5, 6, 8–17]. The motivations for considering dark matter having these masses in the context of the MSSM and in light of experimental constraints are described in Ref. [18] and the references found therein. Recent data from the CoGeNT [19], DAMA/LIBRA [20, 21], and CRESST [22] experiments, on the other hand, hint at the existence of light dark matter (mass of order a few to 10 GeV). Only a few examples exist in the literature which study light dark matter properties, including masses, at hadron colliders, e.g., [23, 24]. In particular, if the dark matter is light, one may not experimentally be able to distinguish it from massless invisible particles, allowing models where neutrinos can fake dark matter signals at a hadron collider [25]. In our analysis, we estimate

¹ We define a $t\bar{t}$ -like event as any decay topology similar to the standard model (SM) leptonic decay of two top quarks: $t\bar{t} \rightarrow W^+bW^-\bar{b} \rightarrow \ell^+\nu_\ell b\ell^-\bar{\nu}_\ell\bar{b}$. We call the top quark the parent particle, the W boson the intermediate particle, and the neutrino is the invisible particle. All of these particles are considered to be potentially massive, while all other particles in the decay chain are assumed to be massless.

how massive the invisible particles must be such that they can be distinguished experimentally at a hadron collider from massless ones.

The outline of our analysis is as follows: in Section II, we define the M_{T2} variable and express the previously-derived [4–6] expressions for its endpoints. In Sections III and IV, we create pseudo-data and use the M_{T2} kink and subsystems methods, respectively, to determine the mass that the invisible particle must have in order to distinguish it from a massless particle at 95% C.L. We do this for various masses of the parent and intermediate particles, and different uncertainties associated with the determination of the M_{T2} endpoints. We conclude and discuss our results in Section V.

II. THE M_{T2} VARIABLE

Consider a general decay chain where a single massive particle, A , with mass m_A , decays to N massless, visible final-state particles and one potentially-massive, invisible particle with physical mass m . The individual three-momenta of the visible particles, \vec{p}_i , are measured, and their four-momenta, p_i^μ , are inferred with the massless approximation.² The invariant mass of the visible system, M_{vis} , is defined as

$$M_{\text{vis}}^2 \equiv P_\mu P^\mu, \quad P^\mu \equiv \sum_i^N p_i^\mu. \quad (1)$$

At a hadron collider, the sum of the transverse momentum of all final-state particles in the event is zero (to a good approximation), and the transverse momentum of the invisible particle, \vec{p}_T , can be inferred. We adopt an ansatz for the mass of the invisible particle, \tilde{m} , and define the transverse mass variable M_T , the square of which is defined as

$$M_T^2(P^\mu, \vec{p}_T; \tilde{m}) \equiv M_{\text{vis}}^2 + \tilde{m}^2 + 2 \left(\sqrt{M_{\text{vis}}^2 + |\vec{P}_T|^2} \sqrt{\tilde{m}^2 + |\vec{p}_T|^2} - \vec{P}_T \cdot \vec{p}_T \right). \quad (2)$$

A distribution of M_T values displays a “kinematic endpoint” or “edge” at the value of m_A when $\tilde{m} = m$.

Consider now an event where a pair of A ’s is created. Each parent particle and their daughters belong to a “branch” or “decay chain”, where we add the label “(1)” and “(2)” to distinguish between the respective decay chains. The two parent particles, $A^{(1)}$ and $A^{(2)}$, eventually decay to $N^{(1)}$ and $N^{(2)}$ visible effectively-massless particles and a potentially-massive invisible particle with mass m .³ The measured missing transverse momentum, \vec{p}_T , is the vector sum of the transverse momenta of the two invisible particles. Because there are two invisible particles in the final state, the M_T variable does not provide information concerning the masses of the particles in the decay chain. However, a generalized M_T variable, called M_{T2} , can be introduced [3], and because we do not know how the transverse momentum is shared between the invisible particles, the square of M_{T2} is defined as

$$M_{T2}^2(\tilde{m}) \equiv \min_{\vec{k}_T^{(1)} + \vec{k}_T^{(2)} = \vec{p}_T} \max \left[M_T^2 \left(P^{\mu(1)}, \vec{k}_T^{(1)}; \tilde{m} \right), M_T^2 \left(P^{\mu(2)}, \vec{k}_T^{(2)}; \tilde{m} \right) \right], \quad (3)$$

where $\vec{k}_T^{(1)}$ and $\vec{k}_T^{(2)}$ are free parameters over which the function is minimized, subject to the constraint $\vec{k}_T^{(1)} + \vec{k}_T^{(2)} = \vec{p}_T$. The distribution of M_{T2} exhibits an endpoint, M_{T2}^{max} , at m_A when $\tilde{m} = m$. If $\tilde{m} \neq m$, the M_{T2} endpoint still exists, but its location does not equal m_A . In general, the change in the value of M_{T2}^{max} as a function of \tilde{m} contains the information of the masses of the particles in the decay chains. A remarkable quality of the M_{T2} variable is, for some topologies, the analytical form that describes M_{T2}^{max} when $\tilde{m} > m$ is different from that when $\tilde{m} < m$. While these functions are continuous for all \tilde{m} , their first derivatives are not, and a “kink” exists in the distribution of $M_{T2}^{\text{max}}(\tilde{m})$ at $\tilde{m} = m$ [5, 6]. By analyzing the shape of the M_{T2}^{max} distribution as a function of \tilde{m} , one can determine, in principle, the masses of the particles in the decay chains.

For the rest of our discussions, we will assume a $t\bar{t}$ -like topology, as shown in Fig. 1: $A^{(i)} \rightarrow B^{(i)} D^{(i)}$, followed by $B^{(i)} \rightarrow C^{(i)} E^{(i)}$, where $i = 1, 2$ and C is considered to be the potentially-massive invisible particle. We make no further assumptions regarding what particle types are D or E , only that they are effectively-massless and their

² The results presented here, of course, also apply for massive visible particles, as long as these are properly identified.

³ It is unnecessary to provide any further details concerning the topology of the decay chain at this point.

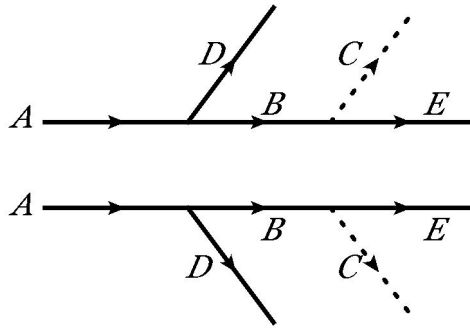


FIG. 1: The decay topology of the pair production of parent particle, A , which decays into two visible effectively-massless final-state particles, D and E , and an invisible potentially-massive particle, C . Here, B is considered to be on-shell.

three-momenta can be reconstructed. Particles A , B , and C have mass m_A , m_B and m_C , respectively, and we assign the ansatz \tilde{m}_C for the mass of the invisible particles. The analytical expressions for $M_{T2}^{\max}(\tilde{m}_C)$ for the $t\bar{t}$ -like topology are, in the limit of no initial-state radiation (ISR) [6, 7],

$$M_{T2}^{\max}(\tilde{m}_C) \equiv \begin{cases} \frac{m_A^2 - m_C^2}{2m_A} + \sqrt{\left(\frac{m_A^2 - m_C^2}{2m_A}\right)^2 + \tilde{m}_C^2}, & \tilde{m}_C \leq m_C, \\ \frac{m_A^2 - m_B^2}{2m_A} + \frac{m_A}{2} \left(1 - \frac{m_C^2}{m_B^2}\right) + \sqrt{\left[\frac{m_A^2 - m_B^2}{2m_A} - \frac{m_A}{2} \left(1 - \frac{m_C^2}{m_B^2}\right)\right]^2 + \tilde{m}_C^2}, & \tilde{m}_C \geq m_C. \end{cases} \quad (4)$$

By fitting the distribution of M_{T2}^{\max} as a function of \tilde{m}_C with the expression for $M_{T2}^{\max}(\tilde{m}_C)$ in Eq. (4), one can simultaneously solve for m_A , m_B , and m_C .

Finding the kinematic endpoint of the M_{T2} distribution can be difficult [26]. The endpoint feature can be obfuscated by decay widths, finite detector resolutions and lack of statistics around the kinematic endpoint. Additionally, it is often experimentally difficult to distinguish different types of final-state jets, e.g., if a reconstructed jet is due to a gluon or quark, so if there are jets in the final state of the pair-produced decay chain, the M_{T2} endpoints can be contaminated with initial-state radiation jets [27, 28]. There can also exist combinatorial ambiguities associated with which jet is to be paired with which decay chain [29–31]. While these experimental issues are crucial and need to be ultimately understood in detail, we assume in this analysis that they only contribute to the overall uncertainty associated with determining the location of an M_{T2} endpoint. This will become clear in the coming sections.

III. M_{T2} KINK METHOD

The determination of $M_{T2}^{\max}(\tilde{m}_C)$ for a given \tilde{m}_C will have an associated uncertainty, σ_E . To study the uncertainties associated with the determination of the mass of the invisible particle, one could consider producing Monte Carlo (MC) events of a $t\bar{t}$ -like topology with a detector simulation and using a procedure to measure the M_{T2}^{\max} distribution as a function of \tilde{m}_C . Because of the significant amount of time it would take to create and analyze such MC samples, we choose to simulate simplified pseudo-data of the $M_{T2}^{\max}(\tilde{m}_C)$ distribution. We take note that the individual values of $M_{T2}^{\max}(\tilde{m}_C)$ are highly correlated between values of \tilde{m}_C that are close together. This is easily understood since the events that populate the M_{T2} kinematic endpoint for a given \tilde{m}_C are mostly the same, regardless of the choice of \tilde{m}_C .⁴ For simplicity, we assume that this correlation does not depend on the physical masses of the decay topology,⁵ and we choose to sample $M_{T2}^{\max}(\tilde{m}_C)$ in 0.25 GeV steps of \tilde{m}_C . We find that a smaller step size of \tilde{m}_C yields endpoints that are too correlated for adjacent values of \tilde{m}_C , and a larger step size would hinder the ability to resolve the position of the kink when it has a value close to zero. When simulating the simplified pseudo-data, one must take care to estimate the positive correlations between M_{T2} endpoint measurements because ignoring to do so would imply infinite precision with which one could determine the $M_{T2}^{\max}(\tilde{m}_C)$ distribution and thus determine the masses of the particles in the decay chain with infinite resolution.

⁴ The endpoint of the M_{T2} distribution is due to a particular momentum configuration of the final-state particles in the decay chains [5, 6].

⁵ In general, highly-correlated values of M_{T2}^{\max} for different values of \tilde{m}_C involve a high percentage of the M_{T2}^{\max} region from “unbalanced solutions” of M_{T2} (the definition of which can be found in Refs [6, 32]).

The full summary of our study of the correlation between $M_{T2}(\tilde{m}_C)$ endpoints can be found in Appendix A. We estimate a nearest-neighbor correlation (NNC) coefficient (as defined in Appendix A) of 0.5 between neighboring $M_{T2}(\tilde{m}_C)$ endpoints for 0.25 GeV steps in \tilde{m}_C .

With this choice of NNC, we generate fifty thousand pseudo-data $M_{T2}^{\max}(\tilde{m}_C)$ distributions for different values of m_C , fitting them with the analytical functions for M_{T2}^{\max} in Eq. (4), for which the physical masses of the decay topology are the fitting parameters. For each fitted distribution of M_{T2}^{\max} , we histogram the fifty thousand best fit values of m_C (which explicitly marginalizes over the uncertainties associated with the m_A and m_B fitting parameters), and from the width of this histogram, we estimate the 95% C.L.⁶ associated with the value of m_C .

To draw similarities from a SM production of $t\bar{t}$ events, i.e., for $m_A = 172$ GeV, $m_B = 80.4$ GeV (while still letting m_C float), the uncertainties of the measurement of m_C given $\sigma_{E_i} = 1$ GeV and $\sigma_{E_i} = 5$ GeV are shown in Fig. 2. From these figures, one can determine what the mass of m_C must be in order to distinguish it from $m_C = 0$ at 95% C.L. If we call this value m_C^{\min} , then $m_C^{\min} \approx 9$ GeV if $\sigma_E = 1$ GeV, and $m_C^{\min} \approx 17$ GeV if $\sigma_E = 5$ GeV. We also estimate m_C^{\min} when $m_A = 500$ GeV and $m_B = 100$ GeV, as shown in Fig. 3, and when $m_A = 500$ GeV and $m_B = 480$ GeV, as shown in Fig. 4.

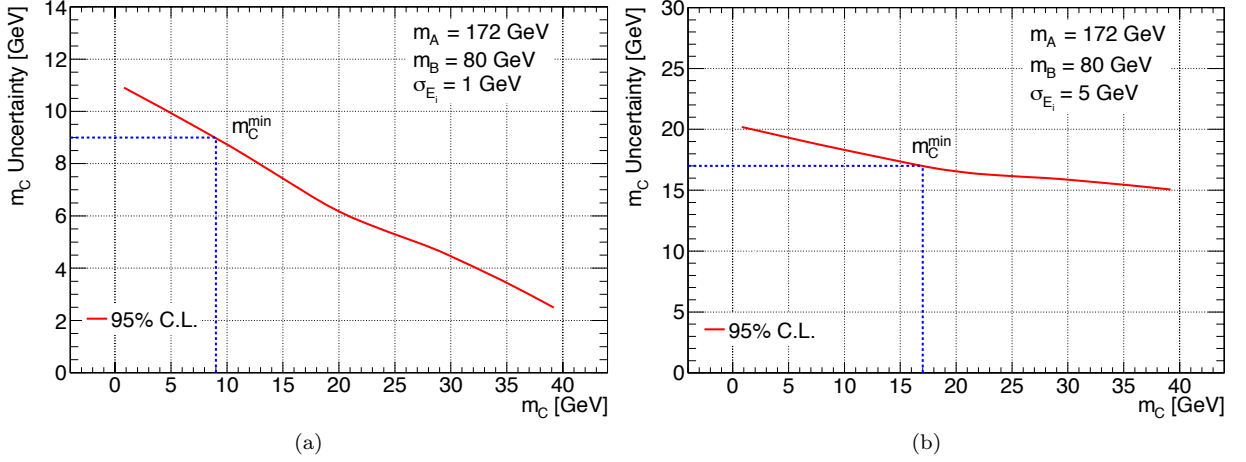


FIG. 2: The 95% C.L. for the mass of m_C for $m_A = 172$ GeV and $m_B = 80.4$ GeV with (a) $\sigma_{E_i} = 1$ GeV and (b) $\sigma_{E_i} = 5$ GeV, using the M_{T2} kink method. The variable m_C^{\min} is the value of mass of m_C at which it can be distinguished from zero at 95% C.L.

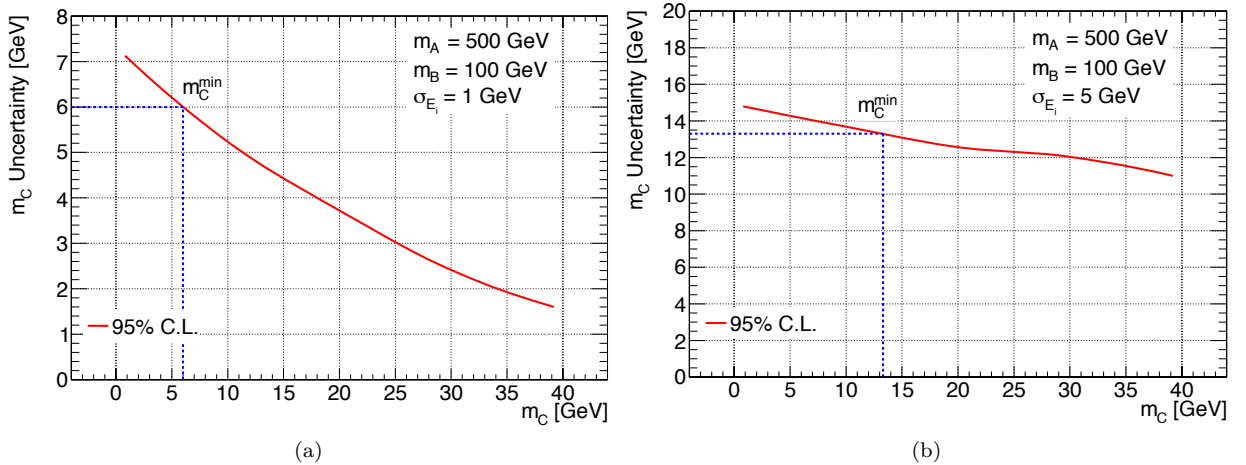


FIG. 3: As in Fig. 2, for $m_A = 500$ GeV and $m_B = 100$ GeV.

⁶ We use the term “C.L.” to describe the uncertainty associated with the sampling method.

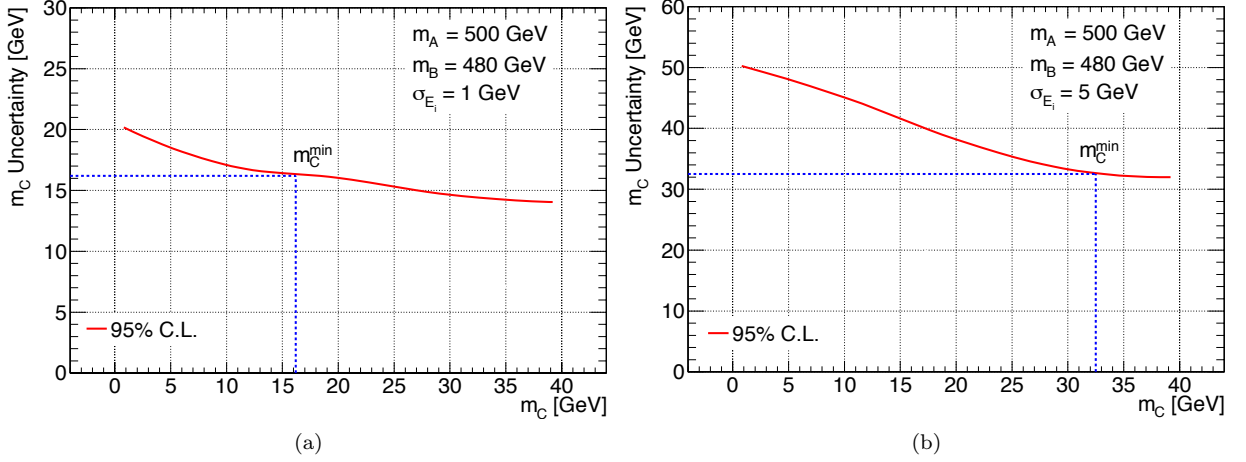


FIG. 4: As in Fig. 2, for $m_A = 500$ GeV and $m_B = 480$ GeV.

IV. M_{T2} SUBSYSTEMS METHOD

To simultaneously measure m_A , m_B , and m_C , the M_{T2} subsystems method relies on the measurement of three independent endpoints: E_{210} ($M_{T2}^{\max}(\tilde{m}_C = 0)$ of the $C^1 E^1 C^2 E^2$ system), E_{221} ($M_{T2}^{\max}(\tilde{m}_C = 0)$ of the $D^1 E^1 D^2 E^2$ system), and E_{im} (endpoint of the invariant mass of the visible $D^1 E^1$ or $D^2 E^2$ systems). These endpoints can be expressed as functions of the physical masses in the decay chain. Following the naming convention in Ref. [7],

$$E_{221} = \frac{m_A^2 - m_B^2}{m_A}, \quad (5)$$

$$E_{210} = \sqrt{\frac{(m_A^2 - m_C^2)(m_B^2 - m_C^2)}{m_A^2}}, \quad (6)$$

$$E_{im} = \sqrt{\frac{(m_A^2 - m_B^2)(m_B^2 - m_C^2)}{m_B^2}}. \quad (7)$$

Given a measurement of the endpoints E_i , where $i = 221, 210$, or im , each with an associated uncertainty, σ_{E_i} , one can, in principle, invert Eqs. (5)-(7) to solve for m_A , m_B , and m_C as a function of the three E_i 's. However, because the measured endpoints may not have exactly the expected values, the system of equations may not be invertible without introducing large uncertainties. Instead of inverting the equations, we choose to perform a χ^2 fit using the measured values of E_i , σ_{E_i} , and the expected values of the endpoints as a function of the physical masses as expressed in Eqs. (5)-(7). This χ^2 function can be minimized with respect to m_A , m_B^2 , and m_C^2 , yielding the best estimates \hat{m}_A , \hat{m}_B^2 , and \hat{m}_C^2 for every set of E_i and σ_{E_i} . In the fit, we allow m_B^2 and m_C^2 to float negative but constrain m_A to be positive. We assume that the uncertainties associated with the three E_i 's are uncorrelated.

To estimate the uncertainties associated with our ability to measure m_C , we generate fifty thousand pseudo-experiments, each with a set of three endpoint measurements, E_i , and each endpoint with the same uncertainty, σ_{E_i} , for simplicity. A χ^2 function is minimized for each pseudo-experiment, negative values of \hat{m}_C^2 are set to zero (since they are unphysical), and the square root of the positive values of \hat{m}_C are histogrammed. We find that the center of this distribution is centered about the physical mass m_C and integrate about this center to find the 95% C.L. associated with the uncertainty of m_C .

In order to compare these results with those found using the M_{T2} kink method, we produce similar plots as in Figs. 2-4, using the M_{T2} subsystems method. These are depicted in Figs. 5-7. We find very similar results for the value of m_C^{\min} between the M_{T2} subsystems and kink methods. This makes us confident that the procedure described in Appendix A is sufficient to simulate the correlations between different M_{T2} endpoints as a function of \tilde{m}_C .

We estimate m_C^{\min} as a function of both m_A and m_B , as shown in Fig. 8, using the M_{T2} subsystems method. We find when the masses of the parent and intermediate particles are close, the value of m_C^{\min} is higher as compared to when m_A and m_B have a large mass difference. We choose not to compute the two-dimension plots of m_C^{\min} using the M_{T2}

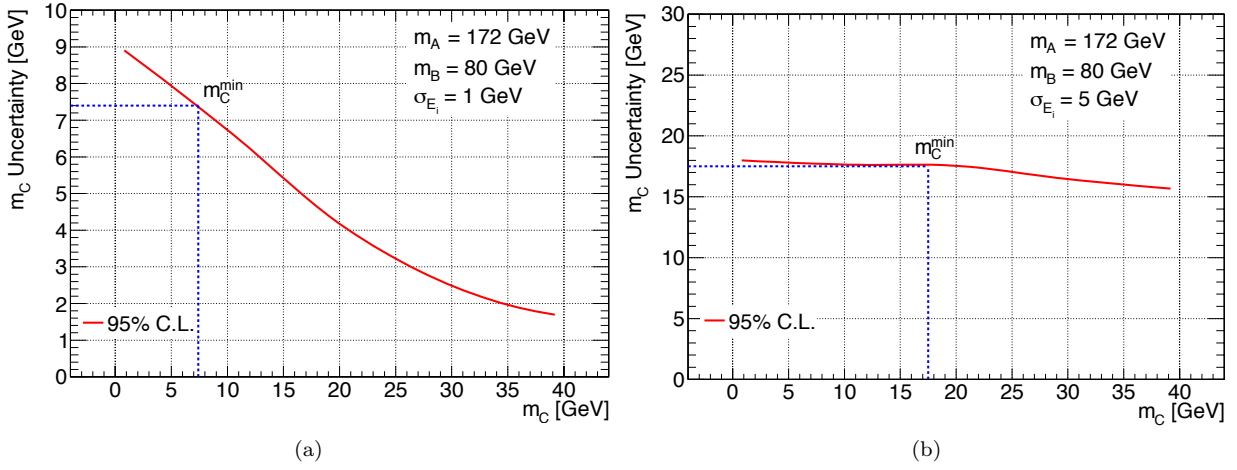


FIG. 5: The 95% C.L. for the mass of m_C for $m_A = 172$ GeV and $m_B = 80.4$ GeV with (a) $\sigma_{E_i} = 1$ GeV and (b) $\sigma_{E_i} = 5$ GeV, using the M_{T2} subsystems method. The variable m_C^{\min} is the value of mass of m_C at which it can be distinguished from zero at 95% C.L.

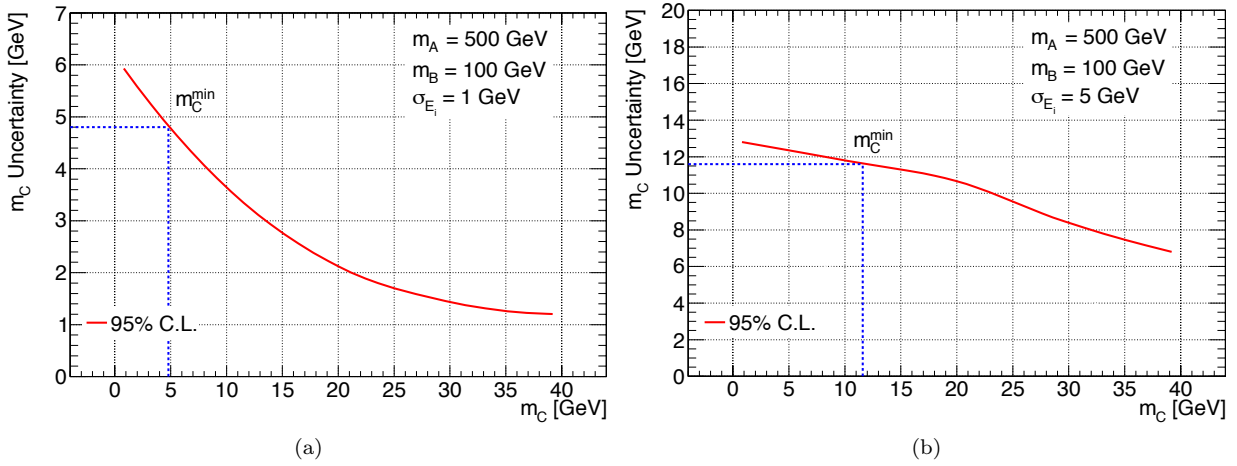


FIG. 6: As in Fig. 5, for $m_A = 500$ GeV $m_B = 100$ GeV.

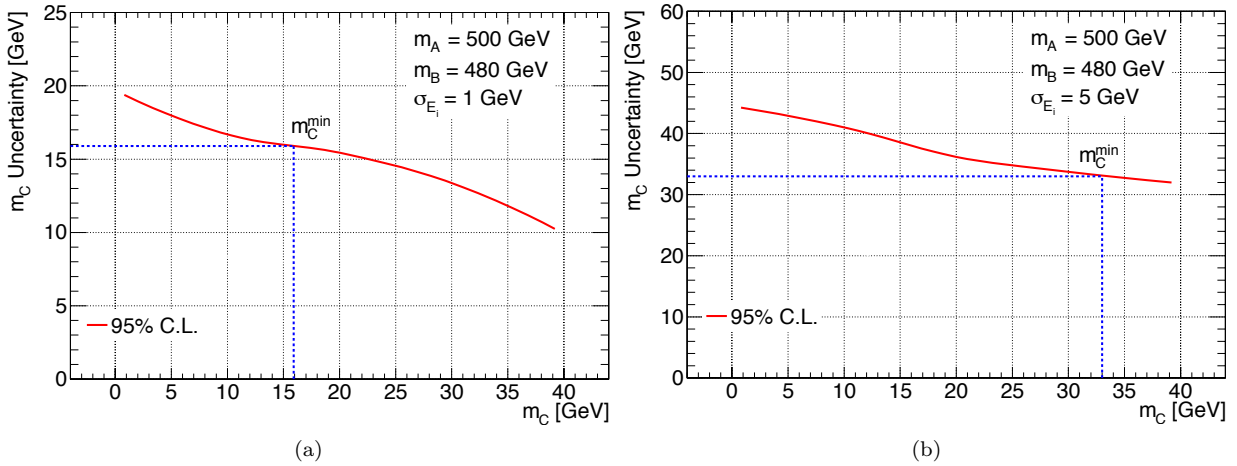


FIG. 7: As in Fig. 5, for $m_A = 500$ GeV $m_B = 480$ GeV.

kink method, as in Fig. 8, since creating the pseudo-data to make the $M_{T2}^{\max}(\tilde{m}_C)$ distributions is computationally expensive, and would require a sizable amount of running time.

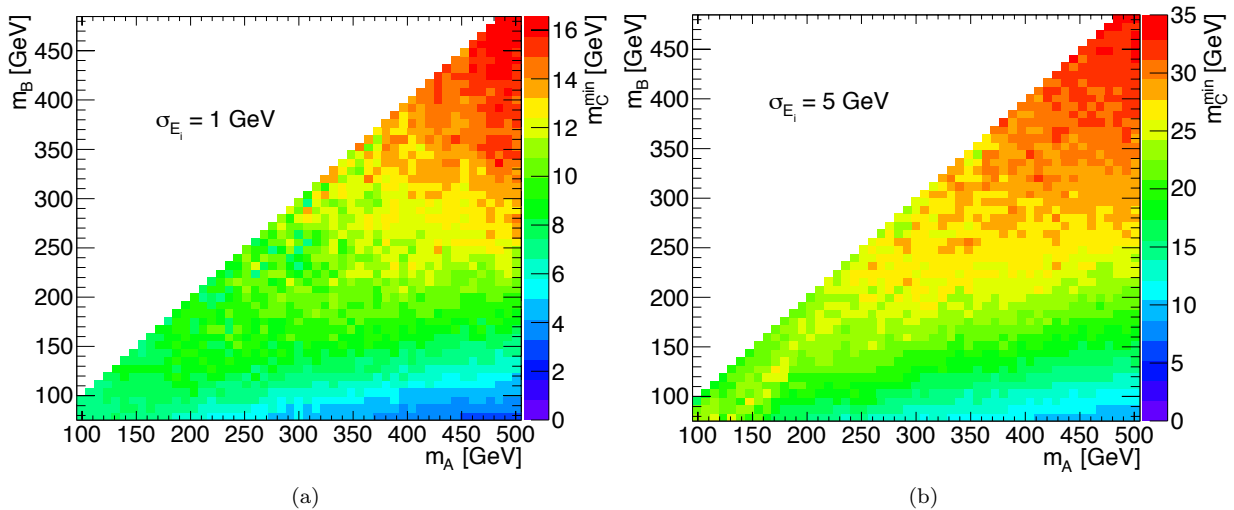


FIG. 8: The values of m_C^{\min} , as a function of m_A and m_B , when (a) $\sigma_{E_i} = 1$ GeV and (b) $\sigma_{E_i} = 5$ GeV using the M_{T2} subsystems method.

V. CONCLUSION

The observation of new physics events with large missing transverse energy at the LHC would potentially serve as evidence for the production of dark matter. A crucial step toward verifying such evidence is the measurement of the masses of the would-be dark matter particles, i.e., the invisible particles. If, say, an excess of invisible particles is discovered and their masses are found to be consistent with zero, one can either conclude that there are new light massive invisible particles, their masses obfuscated by experimental resolution, or that there is new physics in the neutrino sector [25]. As hinted by the CoGeNT [19], DAMA/LIBRA [20, 21], and CRESST [22] experiments, dark matter may have a mass of $\mathcal{O}(10$ GeV). Coincidentally, assuming that dark matter is produced at hadron colliders as the decay product of a $t\bar{t}$ -like event topology and considering reasonable experimental uncertainties, we find that dark matter must have a mass greater than $\mathcal{O}(10$ GeV) such that it can be distinguished from neutrinos at 95% C.L. using M_{T2} -based methods. In general, the uncertainty associated with measuring the mass the invisible particles increases (decreases) as the mass decreases (increases). Our results suggest that, at the LHC, it will prove very challenging to distinguish light dark matter from neutrinos through mass measurements alone if the dark matter weighs around 10 GeV or less.

As seen in Fig. 8, the uncertainty associated with the measurement of the invisible particles' mass increases as the mass m_B of the intermediate particles is close to the mass m_A of the parent particles, and one finds the inverse effect if the intermediate particles are much lighter than the parent particles. In other words, a more precise measurement of the mass of the invisible particles can be made when the intermediate particles have a larger momentum in the center-of-mass frame of the two parent particles. Furthermore, the uncertainty associated with the measurement of the invisible particles' mass also increases as the parent particles' mass increases, for fixed m_B/m_A . These features are due to the fact that the kink structure of the $M_{T2}^{\max}(\tilde{m}_C)$ distribution becomes more pronounced when there is a large mass difference between the parent and intermediate particles. A similar scenario occurs when the intermediate particle is off-shell, such that $m_B > m_A > m_C$, i.e., the kink structure becomes more pronounced [7]. While a more pronounced kink structure will increase the precision at which one can measure the masses of particles involved in a given decay chain, it is not generally expected that it will change the shape of the uncertainty associated with m_C as a function of the physical masses.

The precision associated with measuring the mass of the invisible particles comes from how precisely one can locate the position of the M_{T2} endpoints with a model-independent procedure. Detector resolution, combinatorial ambiguities, and jet contamination are among the many significant obstacles for the precise determination of M_{T2} endpoints. We choose the 1σ Gaussian uncertainties of $\sigma_E = 1$ GeV and $\sigma_E = 5$ GeV to be, respectively, a realistic estimate (compared to, say, reconstructed $t\bar{t}$ final states at the LHC) and a more conservative estimate for the

uncertainties associated with the capabilities of the LHC [33]. If the uncertainty for locating an endpoint is greater than 5 GeV, we expect the precision with which one can measure the invisible particle mass to deteriorate accordingly.

The individual events that populate the region about an M_{T2} endpoint for a given value of the ansatz mass are, to a good approximation, the same events that populate the endpoint for another nearby value of the ansatz mass. As shown in Fig. 9 (see Appendix A), the values of M_{T2}^{\max} are not randomly distributed about the theoretical expectation, and while there are systematic uncertainties associated with M_{T2} endpoint-finding procedure, there can be significant correlations between the measured values $M_{T2}^{\max}(\tilde{m}_C)$ for adjacent values of \tilde{m}_C . For this reason, one cannot simply fit the measured value of M_{T2}^{\max} using Eq. (4) while treating the individual values of M_{T2}^{\max} as independent measurements. In our analysis, we take this correlation into account when fitting with Eq. (4) and marginalize over the other fitting parameters in order to correctly quote the uncertainty on the mass of the invisible particles. The majority of analyses in the literature ignore the correlation between values of M_{T2}^{\max} for adjacent values of \tilde{m}_C , e.g., Refs. [5, 6, 12, 17, 24]. If these correlations are not taken into account when using the M_{T2} kink method, we find that the uncertainties associated with the measured masses are underestimated.

Other M_{T2} -based methods and topologies could have been considered in our analysis. All methods capable of extracting the mass of the invisible particles, however, take advantage of singularities in the kinematic phase space [34, 35]. Though some attention has been paid to other methods that can, in principle, provide more precise mass measurements [36, 37], it is likely that the limitations of the M_{T2} kink and subsystems methods, discussed here in some detail, will be similar to the limitations of other methods as far as determining the mass of light invisible particles is concerned. It is also likely that the features associated with the change in the uncertainty of the invisible particle as the physical masses change are not a consequence of the M_{T2} -based methods we choose, but rather an inherent quality of measuring the mass of invisible particles. As already emphasized, the uncertainty associated with the mass of the invisible particle increases (decreases) as its mass decreases (increases), as can be seen in Figs. 2-7. In addition, as shown in Fig. 8, the uncertainty increases (decreases) as the difference between the mass of the parent and intermediate particles decrease (increase). We believe that these results are independent from the method used to extract the mass of the invisible particles.

Acknowledgments

The authors are grateful to Spencer Chang, Nicholas Eggert, KC Kong, and Konstantin Matchev for useful conversations and feedback. The work of AdG is sponsored in part by the DOE grant # DE-FG02-91ER40684. ACK is supported in part by the Department of Energy Office of Science Graduate Fellowship Program (DOE SCGF), made possible in part by the American Recovery and Reinvestment Act of 2009, administered by ORISE-ORAU under contract no. DE-AC05-06OR23100.

Appendix A: Correlations between M_{T2} endpoints

To understand the correlation between endpoint measurements, we generate a MADGRAPH5 [38] sample of one hundred thousand SM $pp \rightarrow t\bar{t}$ events at $\sqrt{s} = 7$ TeV, where the mass of the top quark is 172 GeV (corresponding to m_A), and the mass of the W is 80.4 GeV (corresponding to m_B). At the generator level, we fit the endpoint of a given M_{T2} distribution with the following four-parameter probability density function:

$$\rho(x; A, k_L, k_R, x_0) = \begin{cases} Ae^{-k_R(x-x_0)}, & x_{\min} < x < x_0, \\ Ae^{-k_L(x-x_0)}, & x_0 < x < x_{\max}, \end{cases} \quad (\text{A1})$$

where x is a dummy variable for the x -axis of an M_{T2} distribution, A is a normalization constant, x_0 is taken to be the location of M_{T2}^{\max} , and k_L and k_R are the exponential slopes on the left and right sides of the kink, respectively. We assume no combinatorial background associated with which jet is associated with which decay branch. The values of x_{\min} and x_{\max} are chosen *a priori* to be certain values about the expected value of M_{T2}^{\max} . While picking values of x_{\min} and x_{\max} based off a theoretical expectation introduces a bias, we are only interested in extracting information concerning a rough estimation of how correlated adjacent endpoint measurements are as a function of \tilde{m}_C . For each $M_{T2}(\tilde{m}_C)$ distribution, we perform an unbinned log-likelihood fit, where the log-likelihood function is defined using events with a value of M_{T2} between x_{\min} and x_{\max} ,

$$\ln \mathcal{L} = \sum_{x_{\min} < x_i < x_{\max}} \ln \rho(x_i; A, m_L, m_R, x_0). \quad (\text{A2})$$

The extremization of $\ln \mathcal{L}$ is performed with MINUIT [39], and the results of the fits are shown in Fig. 9. The uncertainty associated with x_0 is found by marginalizing over the uncertainties for A , m_L , and m_R and varying the log-likelihood about the minimum function by a value of 0.5 as a function of x_0 .

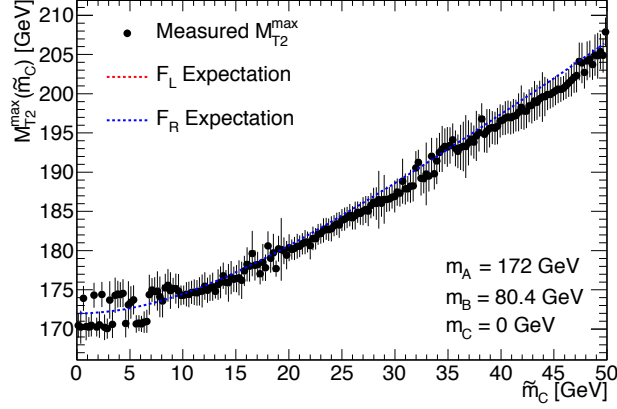


FIG. 9: The fitted endpoints of M_{T2} at the generator level with one hundred thousand events for $m_A = 172$ GeV, $m_B = 80.4$ GeV, and $m_C = 0$ GeV using an unbinned endpoint fitting procedure. The dashed blue and dashed red curves are the theoretical expectations (the red dashed line is not shown since $m_C = 0$ GeV). Note that the points are not randomly distributed about the theoretical expectation.

While this particular MADGRAPH5 sample vastly oversimplifies the type of distributions one would have to work with at a collider experiment, we only wish to extract information concerning the correlation between adjacent endpoints. To estimate the correlation between M_{T2} endpoints and to create pseudo-data, we need to simulate a distribution that properly mimics the one in Fig. 9 while avoiding having to make thousands of MADGRAPH5 samples. To create pseudo-data that contain the correlations we see in Fig. 9, we need to quantify how much each endpoint measurement is correlated with others.

We employ a simplified model of nearest-neighbor correlations. In this method, a single endpoint has its own uncertainty, σ_i , and is positively correlated with the endpoint immediately to the left (except for the left-most endpoint, which is taken to have no correlations with any other endpoint). For simplicity, we consider that all measurements of M_{T2}^{\max} have the same uncertainty, σ_E . We create a covariance matrix, which only includes nearest-neighbor correlations:

$$V_{ij} = \begin{cases} \sigma_E^2, & i = j \\ \text{NNC} \times \sigma_E^2, & |i - j| = 1 \\ 0, & \text{otherwise,} \end{cases} \quad (\text{A3})$$

Here, NNC is the nearest-neighbor correlation factor. With this error matrix, one can iteratively generate pseudo-data that resemble a type of distribution we find with a MADGRAPH5 sample and a simple fitting procedure. We begin with the first point, n_0 , at $\tilde{m}_C = 0$ GeV, allowing it to be Gaussian-distributed about the theoretical expectation, μ_0 , with an error of σ_E . The next point, n_1 , is Gaussian-distributed about the expectation μ_1 with uncertainty σ_E but also is positively correlated to the previous point. These endpoints are random variables sampled from the following probability density function (up to an overall normalization factor):

$$\rho = \begin{cases} e^{-(n_i - \mu_i)^2 / \sigma_E^2}, & i = 0 \\ e^{-(n_i - \mu_i)^2 / \sigma_E^2} \times e^{-(n_i - \mu_i)(n_{i-1} - \mu_{i-1}) V_{i,i-1}^{-1}}, & i > 0, \end{cases} \quad (\text{A4})$$

Examples for the simplified pseudo-data for M_{T2}^{\max} are shown in Fig. 10.

While comparing the MADGRAPH5 and simplified pseudo-data plots by eye is suitable for our purposes, we wish to compare them more quantitatively. We can create a test statistic that estimates how much a given endpoint, n_i , correlates with the endpoint immediately to its left, n_{i-1} :

$$R = \frac{(n_i - \mu_i)(n_{i-1} - \mu_{i-1})}{\sigma_i \sigma_{i-1}}, \quad (\text{A5})$$

where μ_i and μ_{i-1} are the theoretical expectations (given the physical masses of the system) for the M_{T2}^{\max} distribution for bin i and the bin immediately to the left, $i-1$. If each endpoint is statistically uncorrelated with the one immediately

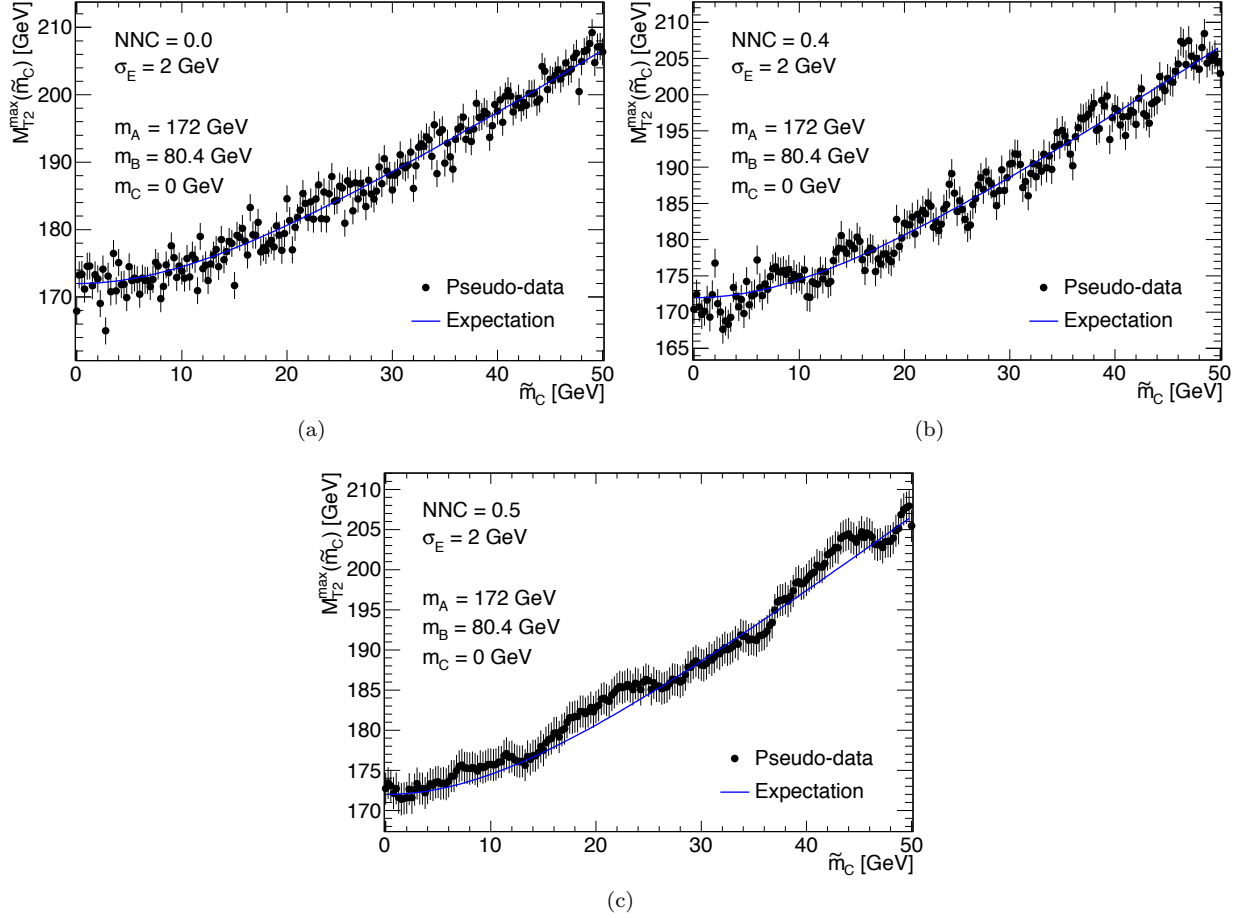


FIG. 10: Sample simplified pseudo-data for M_{T2}^{\max} distribution with for $m_A = 172$ GeV, $m_B = 80.4$ GeV, $m_C = 0$ GeV, $\sigma_E = 2$ GeV, and (a) $NNC = 0$, (b) $NNC = 0.4$, and (c) $NNC = 0.5$.

to the left, the distribution for R should be symmetric about zero. Fig. 11 shows a histogram of the values of R for the MADGRAPH5 sample and the probability density functions for pseudo-data for different values of NNC (these lines are determined by averaging over many generated pseudo-data). Guided by these distributions, we choose a value of $NNC = 0.5$ to perform the study discuss in Sec. III. We choose this value because we interpret that the random jumps in Fig. 9 for $0 < \tilde{m}_C < 10$ GeV are innocuous qualities of our endpoint fitting procedure, and subsequently the histogrammed values of $-2 < R < 0$ in Fig. 11 for the MADGRAPH5 sample are not sampled from the true probability density function for R . Values larger than $NNC = 0.5$ were not studied because they lead to pseudo-data that deviated too much from the theoretical expectation, which is a feature not found in Fig. 9. Finally, we find that the correlation between adjacent values of \tilde{m}_C is not particularly sensitive to the physical masses of the particles in the decay chain, including m_C .

-
- [1] B. Gripaios, Int. J. Mod. Phys. **A26**, 4881 (2011), 1110.4502.
 - [2] A. J. Barr and C. G. Lester, J. Phys. **G37**, 123001 (2010), 1004.2732.
 - [3] C. Lester and D. Summers, Phys. Lett. **B463**, 99 (1999), hep-ph/9906349.
 - [4] A. J. Barr, B. Gripaios, and C. G. Lester, JHEP **0802**, 014 (2008), 0711.4008.
 - [5] W. S. Cho, K. Choi, Y. G. Kim, and C. B. Park, Phys. Rev. Lett. **100**, 171801 (2008), 0709.0288.
 - [6] W. S. Cho, K. Choi, Y. G. Kim, and C. B. Park, JHEP **0802**, 035 (2008), 0711.4526.
 - [7] M. Burns, K. Kong, K. T. Matchev, and M. Park, JHEP **0903**, 143 (2009), 0810.5576.
 - [8] C. B. Park, Phys. Rev. **D84**, 096001 (2011), 1106.6087.
 - [9] K. Agashe, D. Kim, D. G. Walker, and L. Zhu, Phys. Rev. **D84**, 055020 (2011), 1012.4460.
 - [10] M. Adeel Ajaib, T. Li, Q. Shafi, and K. Wang, JHEP **1101**, 028 (2011), 1011.5518.

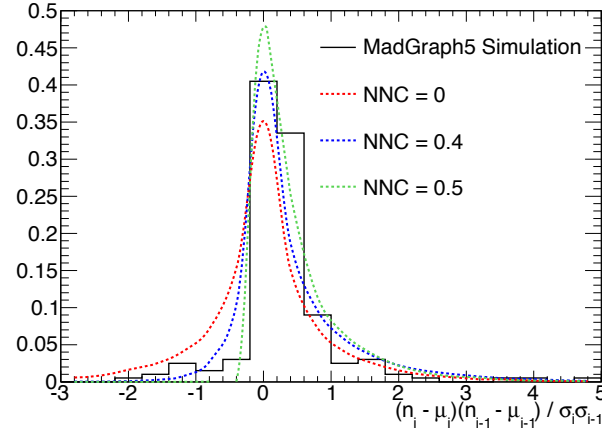


FIG. 11: The variable R as defined in Eq. (A5) for the MADGRAPH5 distribution as in Fig. 9 (black), and three values of the nearest-neighbor correlation factor, NNC. All distributions are normalized to unity.

- [11] C.-Y. Chen and A. Freitas, JHEP **1102**, 002 (2011), 1011.5276.
- [12] K. Choi, D. Guadagnoli, S. H. Im, and C. B. Park, JHEP **1010**, 025 (2010), 1005.0618.
- [13] T. Cohen, E. Kuflik, and K. M. Zurek, JHEP **1011**, 008 (2010), 1003.2204.
- [14] W. S. Cho, K. Choi, Y. G. Kim, and C. B. Park, Nucl. Phys. Proc. Suppl. **200-202**, 103 (2010), 0909.4853.
- [15] J. Alwall, K. Hiramatsu, M. M. Nojiri, and Y. Shimizu, Phys. Rev. Lett. **103**, 151802 (2009), 0905.1201.
- [16] K. Hamaguchi, E. Nakamura, and S. Shirai, Phys. Lett. **B666**, 57 (2008), 0805.2502.
- [17] M. M. Nojiri, Y. Shimizu, S. Okada, and K. Kawagoe, JHEP **0806**, 035 (2008), 0802.2412.
- [18] G. Belanger, S. Biswas, C. Boehm, and B. Mukopadyaya (2012), 1206.5404.
- [19] C. Aalseth et al. (CoGeNT collaboration), Phys. Rev. Lett. **106**, 131301 (2011), 1002.4703.
- [20] R. Bernabei et al. (DAMA Collaboration), Eur. Phys. J. **C56**, 333 (2008), 0804.2741.
- [21] R. Bernabei et al. (DAMA Collaboration, LIBRA Collaboration), Eur. Phys. J. **C67**, 39 (2010), 1002.1028.
- [22] G. Angloher, M. Bauer, I. Bavykina, A. Bento, C. Bucci, et al., Eur. Phys. J. **C72**, 1971 (2012), 1109.0702.
- [23] P. Konar, K. Kong, K. T. Matchev, and M. Park, JHEP **1004**, 086 (2010), 0911.4126.
- [24] G. Belanger, S. Kraml, and A. Lessa, JHEP **1107**, 083 (2011), 1105.4878.
- [25] S. Chang and A. de Gouvêa, Phys. Rev. **D80**, 015008 (2009), 0901.4796.
- [26] D. Curtin, Phys. Rev. **D85**, 075004 (2012), 1112.1095.
- [27] D. Krohn, L. Randall, and L.-T. Wang (2011), 1101.0810.
- [28] M. M. Nojiri and K. Sakurai, Phys. Rev. **D82**, 115026 (2010), 1008.1813.
- [29] P. Baringer, K. Kong, M. McCaskey, and D. Noonan, JHEP **1110**, 101 (2011), 1109.1563.
- [30] K. Choi, D. Guadagnoli, and C. B. Park, JHEP **1111**, 117 (2011), 1109.2201.
- [31] A. Rajaraman and F. Yu, Phys. Lett. **B700**, 126 (2011), 1009.2751.
- [32] A. Barr, C. Lester, and P. Stephens, J. Phys. G **G29**, 2343 (2003), hep-ph/0304226.
- [33] CMS Collaboration, CMS-PAS-TOP-11-027 (2012).
- [34] I.-W. Kim, Phys. Rev. Lett. **104**, 081601 (2010), 0910.1149.
- [35] H.-C. Cheng and Z. Han, JHEP **0812**, 063 (2008), 0810.5178.
- [36] K. T. Matchev, F. Moortgat, L. Pape, and M. Park, Phys. Rev. **D82**, 077701 (2010), 0909.4300.
- [37] P. Konar, K. Kong, K. T. Matchev, and M. Park, Phys. Rev. Lett. **105**, 051802 (2010), 0910.3679.
- [38] J. Alwall, M. Herquet, F. Maltoni, O. Mattelaer, and T. Stelzer, JHEP **1106**, 128 (2011), 1106.0522.
- [39] F. James and M. Roos, Comput. Phys. Commun. **10**, 343 (1975).